RAPID COMMUNICATIONS

PHYSICAL REVIEW B VOLUME 43, NUMBER 16 1 JUNE 1991

Effect of random noise on a mode-locked system

M. F. Crommie,* K. Craig, and M. S. Sherwin
Department of Physics and Center for Nonlinear Science, University of California, Santa Barbara, California 93106

A. Zettl
Department of Physics, University of California, Berkeley, California 94720
and Materials and Chemical Sciences, Division of the Lawrence Berkeley Laboratory, Berkeley, California 94720
(Received 25 February 1991)

We have experimentally added white noise to an analog Josephson-junction simulator in the mode-locked state. The Poincaré sections and power spectra of the analog simulator have been reconstructed from the resultant time-series data. A classical form of noise squeezing is observed. In addition, the power spectra associated with noisy motion about the subharmonic fixed points in the simulator's Poincaré section are found to be Lorentzian in shape. These observations are well accounted for by a theory of noisy mode-locked dynamics recently developed by Wiesenfeld and Satija.

It is well known that nonlinear systems with multiple interacting frequencies display mode-locking behavior.[1] Examples of such systems are periodically driven Josephson junctions,[2] charge-density-wave conductors,[3] and cardiac cells.[4] Less well understood is what influence random noise has on these systems when they are in the mode-locked state.[5] To help explore this phenomenon we have introduced white noise into the drive of a mode-locked Josephson-junction analog simulator and studied the response dynamics through analysis of the resultant Poincaré sections and power spectra.[6]

We find that added noise spreads the mode-locked system into states located preferentially along a (two-dimensional) torus in the three-dimensional phase space of the analog simulator's equations of motion. Subharmonic fixed points in the simulator's Poincaré section tend to spread at different rates along the torus. The subharmonically mode-locked simulator thus displays a form of classical "noise squeezing." The power spectrum associated with the noisy motion about each periodic point is Lorentzian in shape. In general, we find very good agreement between these observations and the recent theory of Wiesenfeld and Satija (WS).[7] However, noise-induced excursions off of the simulator's phase-space attractor necessitate at least some small corrections to the theory of WS.

A phase-locked loop analog simulator of a resistively shunted Josephson junction[8] was externally driven at audio frequencies to display mode-locking behavior. The dimensionless equation of motion of the junction simulator (hereafter referred to as the "junction") is

$$\frac{d^2\theta}{d\tau^2}+G\frac{d\theta}{d\tau}+\sin\theta=i_{\rm dc}+i_{\rm ac}\sin(\Omega_{\rm ac}\tau)+\xi(\tau)\,, \quad (1)$$

where θ is the phase difference across the junction. For our experiments on the 5:2 (external frequency:internal frequency) mode-locked step, $G\approx 2$, setting the junction in the nonhysteretic regime,[2] $i_{\rm dc}\approx 1.31$, $i_{\rm ac}\approx 0.67$, and $\Omega_{\rm ac}\approx 0.29$ (corresponding to 10 kHz). A random voltage from a vacuum-tube white-noise generator (roll-off at 500 kHz) was converted to the random current $\xi(\tau)$ with dimensionless amplitude $2.86\times 10^{-8}\sqrt{\tau}$. Both the voltage across the junction, proportional to $d\theta/d\tau$, and the "supercurrent," proportional to $\sin\theta$, were simultaneously digitized at the ac drive frequency. A plot of $d\theta/dt$ vs $\sin\theta$ "strobed" at the drive frequency defines the Poincaré section.

Figure 1(a) shows the "pumped" dc I-V curve of the junction for $I,V>0$. The vertical axis shows the dc bias current applied to the junction and the horizontal axis shows $\langle(1/2\pi\gamma)d\theta/dt\rangle$, the average voltage across the junction ($\gamma=10$ kHz/V). On the vertical steps in the I-V curve, the junction is mode locked and $\Gamma=(1/2\pi\nu_{\rm drive})\times d\theta/dt$, the winding number, is rational. On the regions of positive slope between the mode-locked steps, the junction is unlocked and Γ is an irrational number. Figure 1(b) shows a Poincaré section of the noisy, pumped dynamics on the 5:2 step ($\Gamma=\frac{5}{2}$). The dotted line shows the actual one-dimensional invariant curve observed experimentally when the junction is biased in the quasiperiodic regime between the mode-locked steps. We refer to this curve as "the circle." The Poincaré section for the 5:2 step is composed of two "noisy" period-2 fixed points (denoted a and b), both of which are spread along the circle by different amounts. The noise in the period-2 fixed point b is "squeezed" compared to the noise in period-2 fixed point a.

Before quantitatively discussing the observed power spectrum and autocorrelation function associated with each periodic point in the Poincaré section, we outline briefly the theory of WS. The theory supposes two conditions, both of which are met in our data.

(1) The system must be strongly mode locked. This means that the noise is sufficiently weak that it can only rarely kick the system out of phase lock and cause the phase to slip. For the data shown in Fig. 1(b), the junction was never kicked out of phase lock.

(2) When a small, random perturbation kicks the system off of the circle, it will relax onto the circle in a time much smaller than the drive period and then relax more

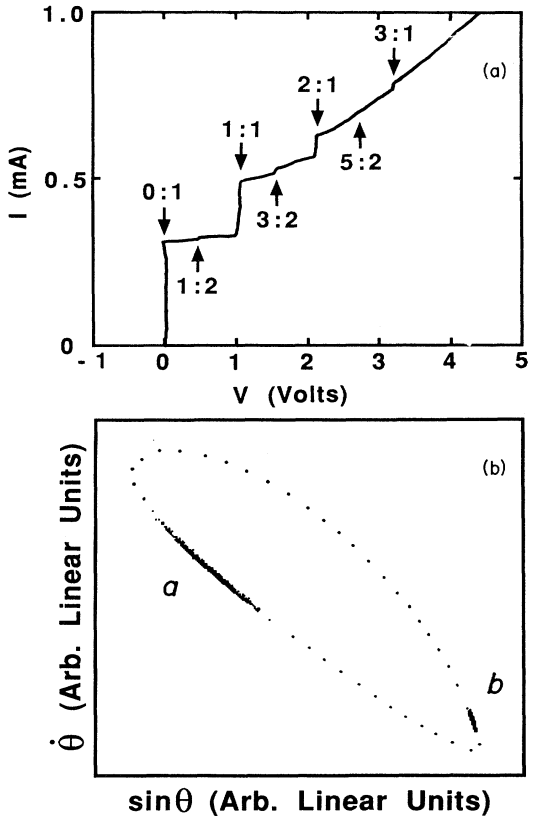

FIG. 1. (a) Mode-locked current vs voltage (I-V) response of the junction simulator. The Shapiro steps are labeled by (internal frequency):(external drive frequency) ratios. (b) Poincaré section when the junction is biased on the 5:2 subharmonic step. The two noisy fixed points are shown, superimposed upon a dotted curve which represents a nearby quasiperiodic orbit.

slowly along the circle towards the fixed point. The dominant excursions around the fixed points are clearly along the circle in Fig. 1(b).

Assuming conditions (1) and (2) are met, WS argue that the Poincaré section of a general mode-locked system can be modeled by a one-dimensional circle map with added noise:

$$\phi_{n+1}=f(\phi_n)+\xi_n\,, \tag{2}$$

where $f(\phi)$ is a 2π periodic function and ξ_n is a random kick. The noise added to the map is white, with zero mean: $\langle\xi_n\rangle=0$ and $\langle\xi_n\xi_m\rangle=\kappa\delta_{n,m}$. If the noiseless map is mode locked with winding number n:1, then the solution to Eq. (1) is a period-1 fixed point, ϕ^*. WS assume that the dynamics of the mode-locked state can be described by a map linearized about the average fixed point:

$$\eta_{n+1}=\lambda\eta_n+\xi_n\,, \tag{3}$$

where $\eta_n=\phi_n-\phi^*$ and $\lambda=(df/d\phi)|_{\phi^*}$. The power spectrum S_k of a time series $\{\eta_n\}$ with N elements is then[9]

$$S_k=(\kappa/N)/(1-2\lambda\cos k+\lambda^2)\,, \tag{4}$$

while the autocorrelation function C_n is predicted to be of the form $C_n\sim\lambda^n$. The model also implies that the distribution of $\{\eta_n\}$ is Gaussian and that κ is determined by the standard deviation about the average fixed point ϕ^* through[9]

$$\sigma=[\kappa/(1-\lambda^2)]^{1/2}\,. \tag{5}$$

WS show that a simple renormalization of time enables one to treat the T fixed points in an n:T subharmonically mode-locked state in the same manner as one would treat an n:1 mode-locked state. We have experimentally studied the case of 5:2 subharmonic mode locking, and so will here concentrate on applying the results of WS to the n:2 mode-locked state. In this situation, Eq. (1) has two period-2 fixed points, while the second-iterate map, $f^2(\phi)$, has two period-1 fixed points, ϕ^{*a} and ϕ^{*b}. (Hereafter, these period-2 fixed points will be referred to simply as "fixed points.") Two new time series, $\{\phi^a_{2n}\}$ and $\{\phi^b_{2n}\}$, can be created by taking the time-ordered set of every second point of the initial time series, $\{\phi_n\}$. In the presence of noise, the second-iterate map can also be linearized, and a power spectrum can be calculated for deviations η^a_{2n} and η^b_{2n} about each average fixed point. The power spectra of $\{\eta^a_{2n}\}$ and $\{\eta^b_{2n}\}$ are of the same form as Eq. (3), but with κ replaced by a renormalized parameter:

$$\kappa'_{a,b}=\kappa(1+\lambda^2_{b,a}) \tag{6}$$

[where $\lambda_a=(df/d\phi)|_{\phi^{*a}}$ and $\lambda_b=(df/d\phi)|_{\phi^{*b}}$], λ replaced by the new stability parameter, $\Lambda=\lambda_a\lambda_b$, and k replaced by $2k$ on the right-hand side. The autocorrelation functions of both $\{\eta^a_{2n}\}$ and $\{\eta^b_{2n}\}$ are shown by WS to fall exponentially with identical decay rates:

$$C^{a,b}_{2n}\propto\Lambda^{2n}\,. \tag{7}$$

The noise strength at each fixed point, however, as seen from Eq. (6), can be very different. For example, if $\lambda_a<\lambda_b$, the fixed point a "squeezes" the noise seen by fixed point b and fixed point b appears more quiet ($\kappa'_b<\kappa'_a$).

In order to quantitatively apply the theory of WS to our results, the data for the $\Gamma=\frac{5}{2}$ Poincaré section were reparametrized to reduce the two-dimensional time series of $(\sin\theta_n,\ d\theta_n/dt)$ pairs to a one-dimensional time series $\{\phi_n\}$. We chose the simplest of several possible reparametrization schemes: The angle $\phi_n=\tan^{-1}[(d\theta_n/dt)/\sin\theta_n]$ was assigned to each $(\sin\theta_n,\ d\theta_n/dt)$ pair in the Poincaré section. The origin was chosen to lie along the perpendicular bisector of the spread in the fixed points in order to gain the maximal angular resolution of the least-stable directions. As prescribed by WS, two experimental time series, $\{\eta^a_{2n}\}$ and $\{\eta^b_{2n}\}$, were generated by subtracting the appropriate average fixed point, $\phi^{*a,b}$, from each of the two, out-of-phase time series $\{\phi_{2n}\}$ and $\{\phi_{2n+1}\}$.

Figure 2 shows the autocorrelation function, $C^{a,b}_{2n}$, of the two time series, $\{\eta^{a,b}_{2n}\}$, about the $\Gamma=\frac{5}{2}$ fixed points (marked a and b, respectively). Except for the excessive autocorrelation at $n=0$ for fixed point b, the logarithm of the autocorrelation functions of the time series for both fixed points lie on straight lines with identical slopes. This figure bears out two of the predictions of WS. First, the autocorrelation function of the two time series $\{\eta^{a,b}_{2n}\}$ is shown to decay exponentially. And second, the decay rate

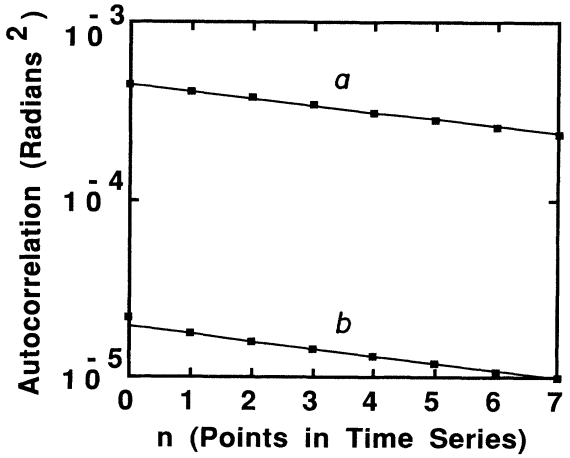

FIG. 2. Discrete points show the autocorrelation function of $\{\eta^a_{2n}\}$ and $\{\eta^b_{2n}\}$ (fixed points a and b, respectively). Solid lines show least-squares linear fits to data.

of the autocorrelation function is identical for each fixed point. One can extract the stability parameter of the $\Gamma = \frac{5}{2}$ subharmonic step, $\Lambda \approx 0.9$, from this decay rate using Eq. (7).

Figure 3 shows the power spectra of the time series about each fixed point on the $\Gamma = \frac{5}{2}$ step. The solid lines show the experimental power spectra, calculated from the time series data using a fast Fourier transform. The power spectra are Lorentzian and extend out to $\omega = \pi$, the normalized Nyquist frequency. As expected, the power spectrum of the wider fixed point a is higher in magnitude than that of the smaller fixed point b—despite the fact that the autocorrelation functions corresponding to the two fixed points decay at identical rates. The dashed curves in the figure are the theoretical fits to the data using Eq. (4) (modified for two fixed points as explained earlier). Λ and $\kappa'_{a,b}$ are obtained for the fits using Eqs. (5) and (7), and there are no free parameters. The agreement between the theoretical and experimental power spectra is excellent at all frequencies for fixed point a, and at low frequencies for fixed point b. The theory underestimates the power spectrum at high frequencies for fixed point b.

The experimental excesses in both the high-frequency power spectra and the $n=0$ autocorrelation function of fixed point b are small deviations from excellent general agreement between the theory of WS and our observations. These differences can both be explained from the fact that while WS consider the slow relaxation *along* the circle, they neglect the effect of fast relaxation *onto* the circle. In general, the Poincaré section of the junction's motion reflects both of these relaxation rates. The two relaxation directions are not necessarily orthogonal in the $(\sin\theta, d\theta/dt)$ plane. Hence, when a center is chosen to convert the data points to angles, even if it is chosen to be along the perpendicular bisector of the fixed point (i.e., perpendicular to the slow rate of relaxation along the circle), the angular data will still contain angular displacements with components along both the slow axis *and* the fast axis (see Fig. 4). For fixed point a, the fast axis was projected out and both autocorrelation and power spectrum are well fit by the slow relaxation rate considered by WS. However, the fast axis makes a contribution to the dynamics near fixed point b. Due to the discreteness of the autocorrelation function, we are unable to accurately measure the relaxation rate of the fast direction. The fast relaxation-rate component of the autocorrelation vanishes in less than one cycle of drive, and hence before $n=1$. However, no matter how fast the relaxation in this direction is, it will always increase at least the zeroth point of the autocorrelation, as this correlates the data to itself without any time delay. This causes the autocorrelation function to decay faster as n goes to zero than for longer times. If one calculates Λ for fixed point b using only the first two points of the autocorrelation function and combines this with Eq. (4), then one obtains a much better

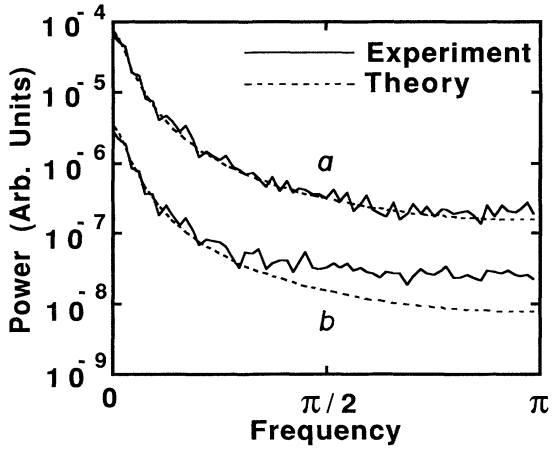

FIG. 3. Solid lines show the experimental power spectra of the phase about fixed points a and b. Dashed lines show the theoretical fits using Eq. (3). The deviation of fixed point b from theory at high frequencies is discussed in the text.

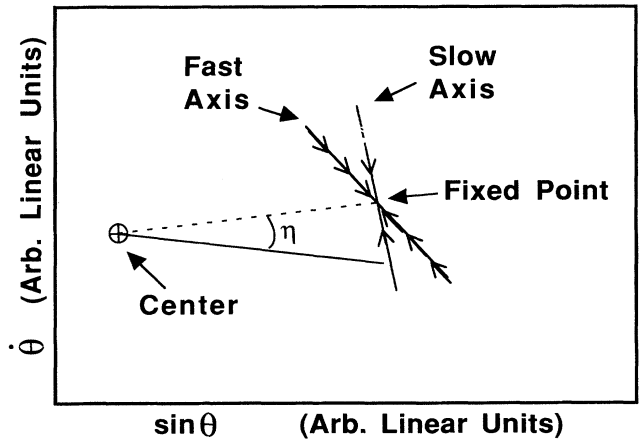

FIG. 4. The geometry involved in collapsing a two-dimensional Poincaré-section data point into a single angle. Note that if the two relaxation directions are not orthogonal, then a general choice of center will project out angles relaxing with both fast and slow rates.

theoretical fit to the high-frequency end of the experimental power spectrum. The fit at the low-frequency end, however, worsens. In general, the power spectrum cannot be perfectly fit by a single relaxation rate.

We have shown that the noisy circle map can indeed make nontrivial, quantitative predictions about mode-locked systems with noise. The predictions are nearly exact if the fast relaxations can be projected out during the parametrization of angles. This result supports the far-reaching claim that the essential dynamics of a real physical system whose behavior is dictated by Eq. (1) can be captured by the discretized circle map with added white noise [Eq. (2)]. An analysis like the one used in this paper may thus be used to determine whether various mode-locking systems can, for some parameters, be modeled by a circle map. One particularly important candidate for such a study is nonlinear charge-density-wave conduction, where the relevance of any circle map or low-dimensional description is a topic of great interest.[10]

We would like to thank J. Levy, C. Tang, K. Wiesenfeld, J. Carlson, and A. Landsberg for stimulating discussions and suggestions. K.C. and M.S.S. were supported by NSF Grant No. DMR 89-01651. M.F.C. and A.Z. were supported in part by NSF Grant No. DMR 84-00041. M.F.C. received additional support from the Center for Nonlinear Science of the Quantum Institute at the University of California at Santa Barbara.

---

*Permanent address: Department of Physics, University of California at Berkeley, Berkeley, CA 94720.

[1]See, for example, M. H. Jensen, P. Bak, and T. Bohr, Phys. Rev. A **30**, 1960 (1984); T. Bohr, P. Bak, and M. H. Jensen, *ibid.* **30**, 1970 (1984); P. Bak, Phys. Today **39** (12), 38 (1986).

[2]A. Barone and G. Paterno, *Physics and Applications of the Josephson Effect* (Wiley, New York, 1982).

[3]For a recent review, see G. Grüner, Rev. Mod. Phys. **60**, 1129 (1988).

[4]M. R. Guevara, L. Glass, and A. Shrier, Science **214**, 1352 (1981).

[5]M. S. Sherwin and A. Zettl, Phys. Rev. B **32**, 5536 (1985).

[6]The construction of stochastic return maps for stochastic ordinary differential equations is discussed by E. Knobloch and J. B. Weiss, in *Noise in Nonlinear Dynamical Systems,* edited by F. Moss and P. V. McLintock (Cambridge Univ. Press, Cambridge, 1989), Vol. 2; J. B. Weiss and E. Knobloch, J. Stat. Phys. **58**, 863 (1990).

[7]K. Wiesenfeld and I. Satija, Phys. Rev. B **36**, 2483 (1987).

[8]The simulator used here is modeled after the JA-100 Josephson-Junction Analog Simulator, Philipp-Gillette and Associates.

[9]Equations (3) and (4) are corrected versions of equations from WS (Ref. 7).

[10]S. N. Coppersmith and P. B. Littlewood, Phys. Rev. Lett. **57**, 1927 (1986).